Supplement of Biogeosciences, 23, 1527–1544, 2026
https://doi.org/10.5194/bg-23-1527-2026-supplement

Biogeosciences Open Access EGU

Supplement of

Nutrient flows and biogeomorphic feedbacks: linking seabird guano to plant traits and morphological change on sandy islands

Floris F. van Rees et al.

Correspondence to: Floris F. van Rees (floris.van.rees@nioz.nl)

S1 Supplementary figures and tables

Table S1: Number of breeding pairs per species per islands.

	Zuiderduin	Rottumerplaat	Rottumeroog	Richel	Griend
Larus argentatus and Larus fuscus	796	4519	794	687	1270
Chroicocephalus ridibundus	13				5282
Phalacrocorax carbo	267			64	
Larus canus	13		45		
Thalasseus sandvicensis					2797
Platalea leucorodia					54
Sterna paradisaea					67
Sterna hirundo					312

Table S2: Contributions and loadings per environmental variable to the primary PC axes that explain at least 85% of total variance.

	Contributions (%)		Loadings	
	PC1	PC2	PC1	PC2
Distance from coast	32	36	0.56	-0.60
Soil organic matter	52	0	0.72	0.03
Mean Elevation in 2022	16	64	-0.40	-0.80

Table S3: Contributions and loadings per vegetation trait to the primary PC axes that explain at least 85% of total variance.

	Contributions (%)			Loadings		
	PC1	PC2	PC3	PC1	PC2	PC3
C:N ratio	3	48	1	-0.18	-0.69	-0.08
C	26	0	11	-0.51	-0.04	-0.33
N	1	49	2	-0.10	0.70	-0.12
Vegetation height	33	0	10	-0.58	-0.05	0.31
Vegetation root depth	14	1	46	-0.37	0.08	-0.68
Vegetation biomass	23	2	31	-0.48	0.16	0.56

Table S4: Number of cells, Coordinates and descriptive statistics of the five islands analysed in this study. Descriptive statistics of NDVI, GI and Z are given for the years 2022 and 2021 and displayed as (Mean ± SD).

Variable	**Zuiderduin**	**Richel**	**Rottumeroog**	**Rottumerplaat**	**Griend**
Number of cells	68279	10979	128465	501266	79591

Area (ha)	61	10	116	451	72
Longitude	53°31'0"N	53°17'50"N	53°32'25"N	53°32'30"N	53°15'55"N
Latitude	6°35'0"E	5°8'5"E	6°34'55"E	6°28'51"E	5°15'15"E
$NDVI_{2021}$	0.311 ± 0.212	0.334 ± 0.153	0.332 ± 0.186	0.343 ± 0.199	0.461 ± 0.180
$NDVI_{2022}$	0.312 ± 0.180	0.328 ± 0.156	0.327 ± 0.173	0.302 ± 0.189	0.442 ± 0.200
GI_{2021} (d^{-1})	0.001 ± 0.001	0.002 ± 0.002	0.002 ± 0.001	0.001 ± 0.001	0.003 ± 0.001
GI_{2022} (d^{-1})	0.001 ± 0.001	0.002 ± 0.001	0.001 ± 0.001	0.001 ± 0.001	0.002 ± 0.001
Z_{2021} (m)	1.437 ± 0.425	1.517 ± 0.343	2.113 ± 1.042	1.858 ± 1.095	1.569 ± 0.990
Z_{2022} (m)	1.426 ± 0.408	2.210 ± 0.734	2.210 ± 1.098	1.908 ± 1.126	1.866 ± 0.760

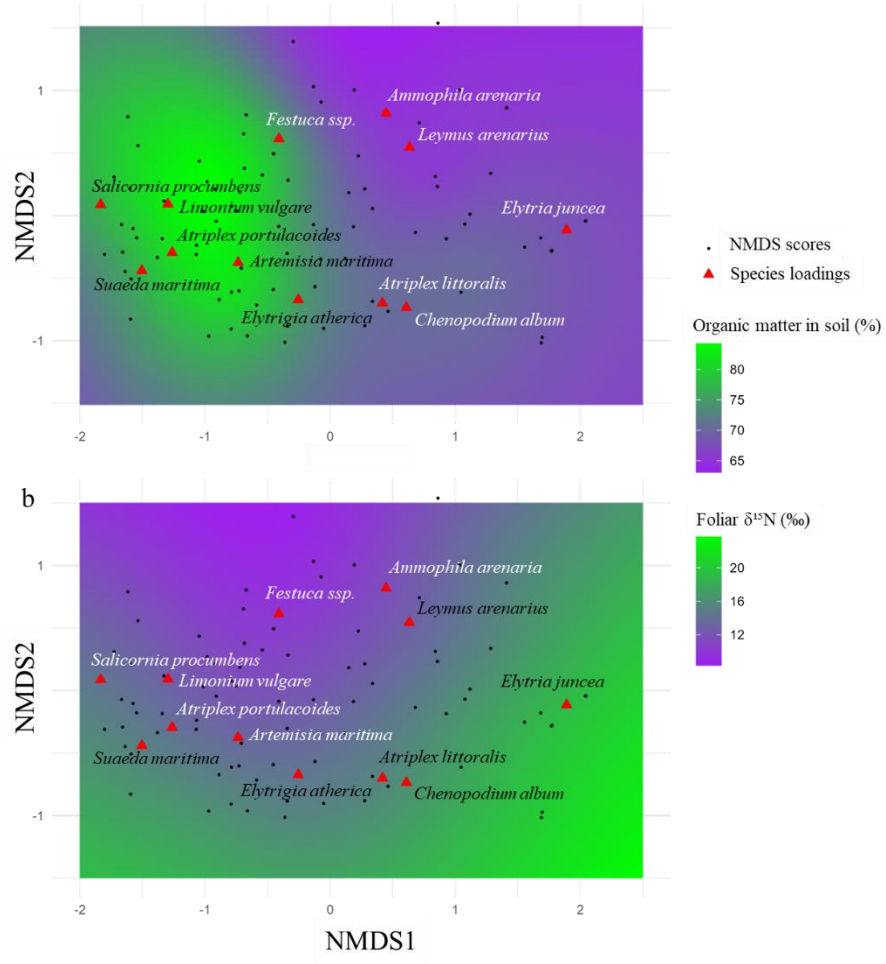

Fig. S1: Prediction of organic matter in the soil (a), and foliar $\delta^{15}N$ (b) based on NMDS scores of plot locations. Here, organic matter and foliar $\delta^{15}N$ values are explained by a smoothed interaction effect between NMDS1, and NMDS2 (s(NMDS1,NMDS2)), $p<0.05$. We solved for larger scale spatial autocorrelation by a tensor smoother on coordinates (te(X,Y)), $p<0.05$. Smoothers were performed by GAMs from the mgcv package in R (Wood & Augustin, 2002), however this was term was not used for prediction purposes, only for improving the accuracy of the s(NMDS1,NMDS2) smoother.

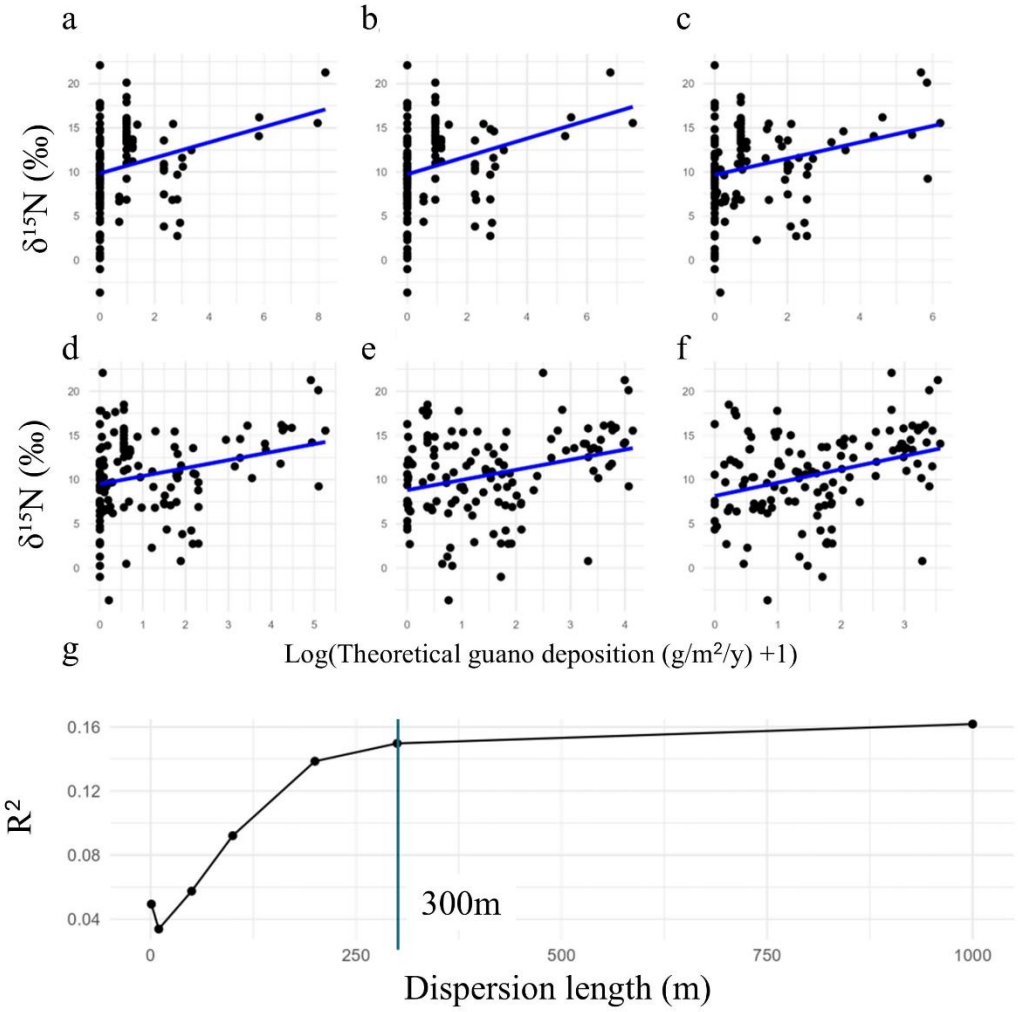

Fig. S2: Relationship between $\delta^{15}N$ and theoretical guano deposition computed by the data-informed model for different dispersion lengths (1, 10, 50, 100, 200, 300, and 1000 m) for panels A-F respectively. Panel G shows the change of the R^2 as a function of the dispersion length.

Table S5: Summary of posterior distribution of main effects as described by mean, standard deviation (SD), 0.025 and 0.975 quantiles.

	GI-based			
Predictor	mean	SD	0.025 quantile	0.975 quantile
(Intercept)	0.131	0.035	0.062	0.2
Log(Guano+1)	0.05	0.025	0.002	0.098
Vegetation Change (ΔGI or ΔNDVI)	-0.038	0.012	-0.061	-0.014
Vegetation State in 2021 (GI or NDVI)	-0.013	0.011	-0.036	0.009
Elevation (2021)	-0.08	0.007	-0.095	-0.066
Island (Richel)	0.731	0.145	0.448	1.015
Island (Rottumeroog)	0.087	0.095	-0.099	0.273
Island (Rottumerplaat)	-0.181	0.078	-0.334	-0.028

Island (Zuiderduin)	-0.258	0.103	-0.459	-0.056
Log(Guano+1) × Vegetation Change	0.011	0.005	0	0.021
Vegetation Change × Richel	-0.034	0.015	-0.064	-0.004
Vegetation Change × Rottumeroog	0.11	0.021	0.069	0.151
Vegetation Change × Rottumerplaat	0.033	0.017	0	0.067
Vegetation Change × Zuiderduin	0.014	0.017	-0.02	0.047
	NDVI-based			
Predictor	mean	SD	0.025 quantile	0.975 quantile
(Intercept)	0.134	0.042	0.052	0.215
Log(Guano+1)	0.037	0.028	-0.019	0.092
Vegetation Change (ΔGI or ΔNDVI)	0.037	0.026	-0.013	0.088
Vegetation State in 2021 (GI or NDVI)	0.011	0.014	-0.018	0.039
Elevation (2021)	-0.081	0.007	-0.096	-0.067
Island (Richel)	0.805	0.169	0.474	1.136
Island (Rottumeroog)	0.074	0.113	-0.146	0.295
Island (Rottumerplaat)	-0.201	0.093	-0.383	-0.019
Island (Zuiderduin)	-0.292	0.123	-0.532	-0.051
Log(Guano+1) × Vegetation Change	-0.033	0.01	-0.052	-0.013
Vegetation Change × Richel	-0.187	0.034	-0.253	-0.121
Vegetation Change × Rottumeroog	-0.029	0.036	-0.1	0.042
Vegetation Change × Rottumerplaat	-0.054	0.032	-0.117	0.01
Vegetation Change × Zuiderduin	0.002	0.029	-0.055	0.058

Table S6: Scaling factors for the z-standardization for the INLA analysis.

Variable	Mean	SD
Log(Guano($g/m^2/y$)+1))	0.866	0.811
GI in 2021 (d^{-1})	0.002	0.001
NDVI in 2021 (-)	0.321	0.191
ΔGI (d^{-1})	0.000	0.001
ΔNDVI (-)	-0.029	0.082
Elevation (2021) (m)	1.829	1.044

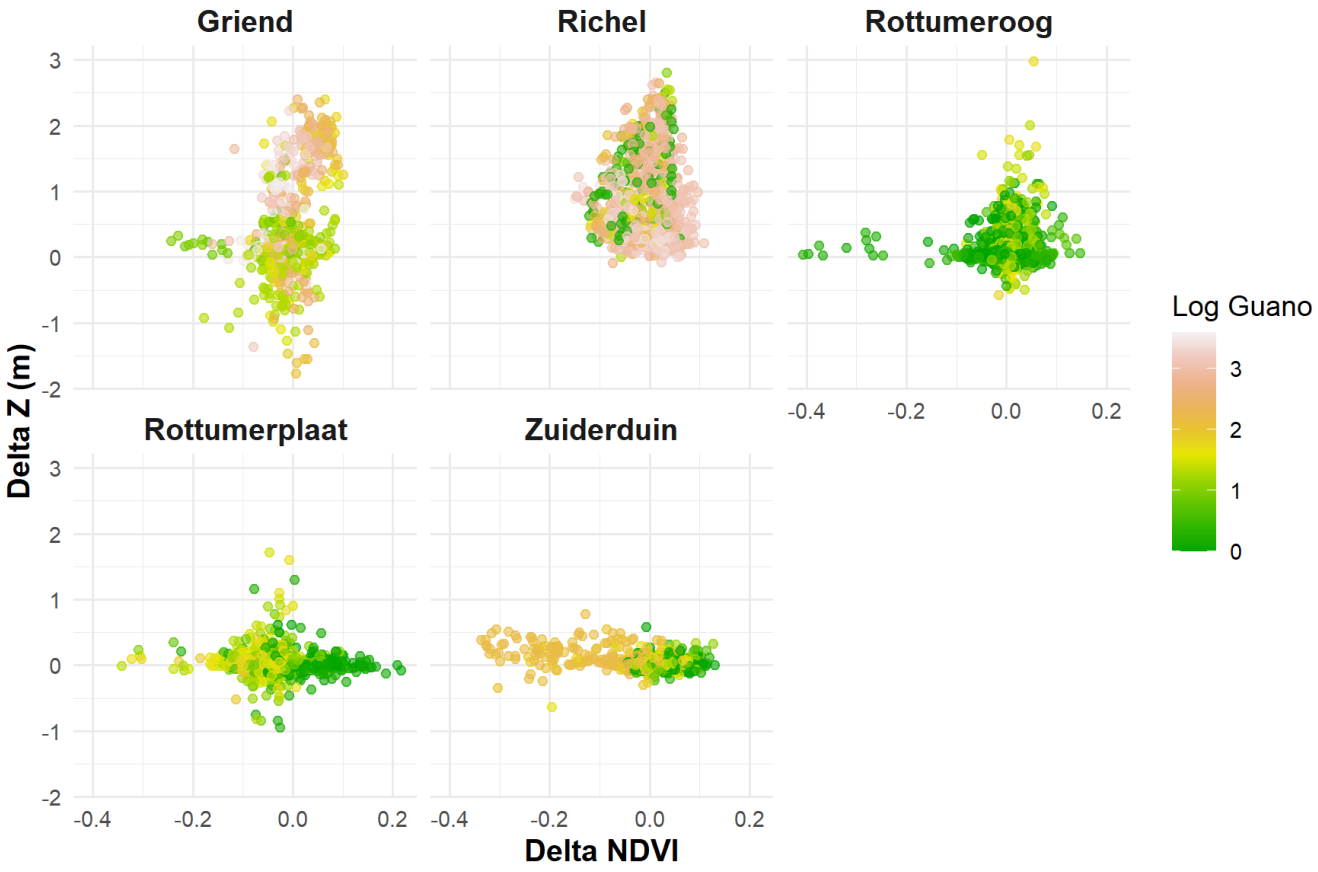

Fig. S3: Relationships between delta Z (m) (change in elevation), and delta NDVI (change in vegetation presence), per island. Delta's are computed based on the difference between 2022 and 2021. The color expresses log-transformed guano deposition in g/m^2/y on the original scale.

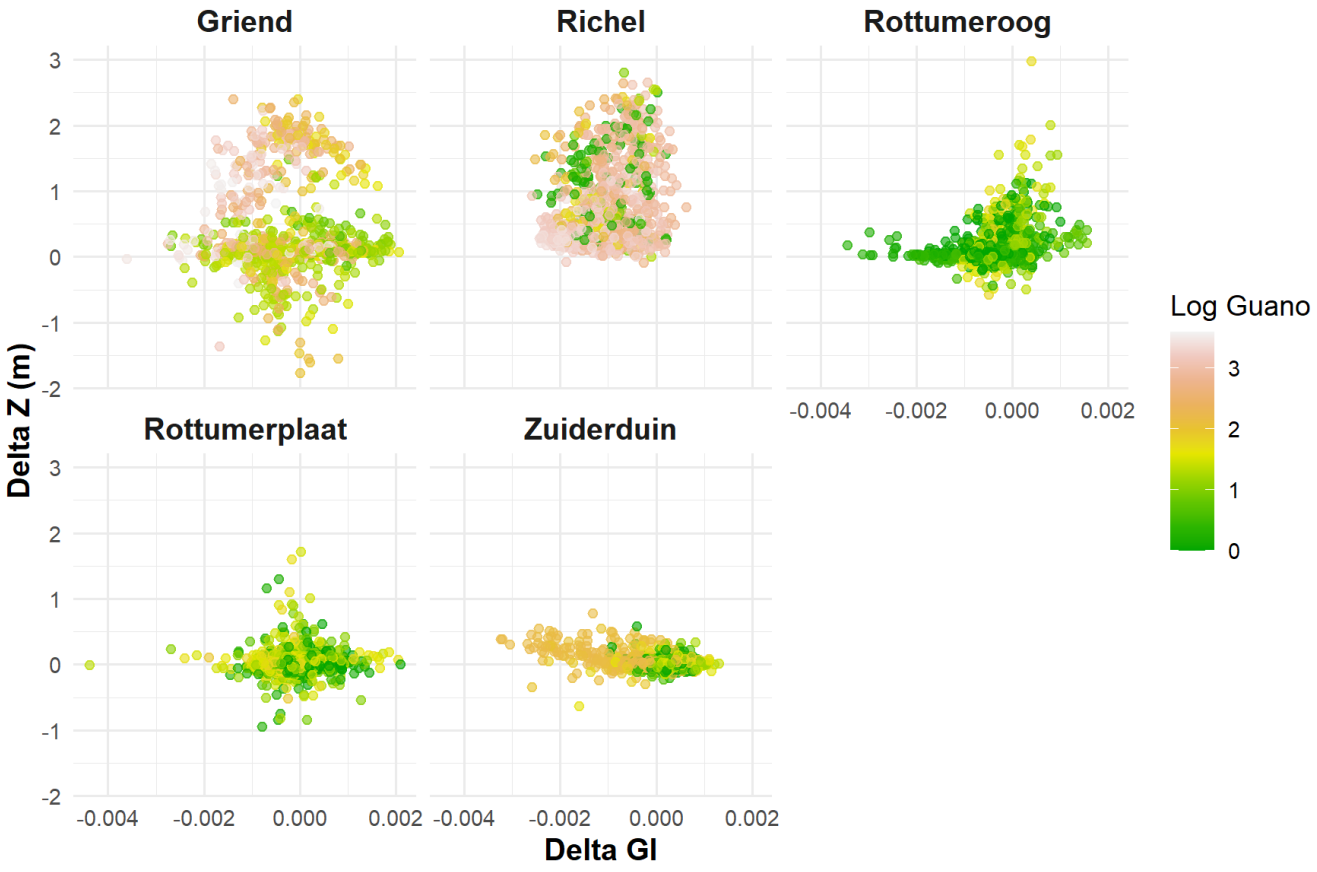

Fig. S4: Relationships between delta Z (m) (change in elevation), and delta GI (change in vegetation presence), per island. Delta's are computed based on the difference between 2022 and 2021. The color expresses log-transformed guano deposition in g/m²/y on the original scale.

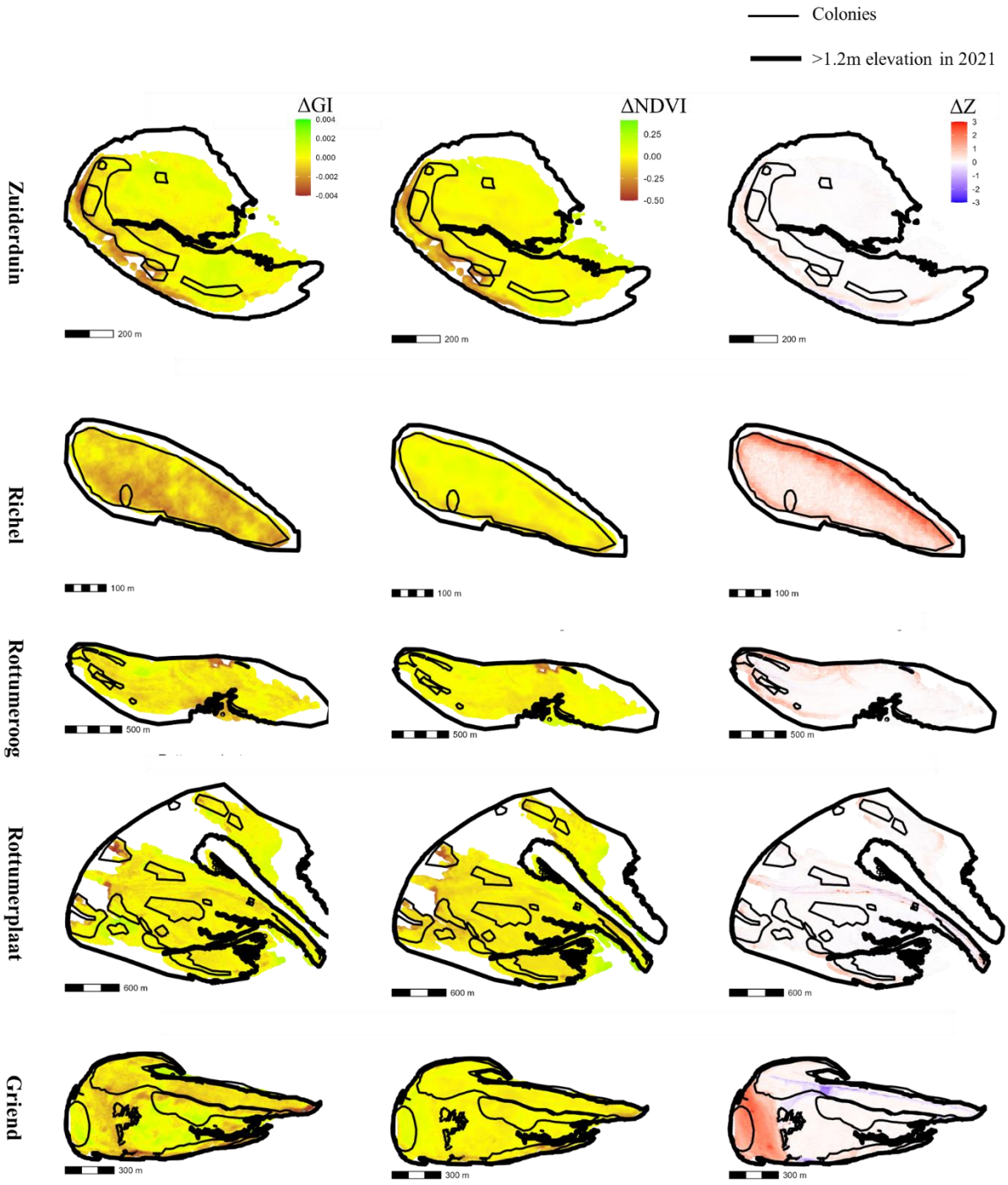

Fig. S5: Spatially explicit values of ΔGI, ΔNDVI, and ΔZ.

S2 Model validation

S2.1 Prior Sensitivity Analyses

We evaluated the sensitivity of model inference to prior assumptions for the spatial random field, specified using Penalized Complexity (PC) priors for a Matérn SPDE representation. For the reference models presented in the manuscript, we assumed a median spatial correlation range of 300 m, expressed as $P(\rho < 300\ \text{m}) = 0.5$, corresponding to the scale of the smallest island (Richel). The

marginal standard deviation of the spatial field was assigned a PC prior $P(\sigma > 1) = 0.1$, allowing substantial spatial variation while penalizing overly complex spatial structure.

To assess prior sensitivity, we varied both spatial hyperparameters. First, we imposed a substantially shorter-range prior ($P(\rho < 50\ \mathrm{m}) = 0.5$) while retaining the original marginal standard deviation prior. Under this alternative specification, posterior estimates of the spatial range and field standard deviation remained essentially unchanged (GI-based model: posterior range ≈ 175 m, spatial SD ≈ 0.30; NDVI-based model: posterior range ≈ 205 m, spatial SD ≈ 0.30), indicating that spatial scale inference was driven primarily by the data rather than the prior.

Second, we evaluated sensitivity to the assumed magnitude of spatial variation by applying a more restrictive prior favoring weak spatial effects ($P(\sigma > 0.1) = 0.5$) while keeping the reference range prior. This prior strongly penalizes large-amplitude spatial fields. Again, posterior estimates of both

spatial hyperparameters and fixed-effect coefficients were nearly identical to those obtained under the reference prior for both models.

Posterior estimates for all fixed main effects and interaction terms were stable across all prior scenarios (Fig. S), indicating that inference on covariate effects was robust and not driven by the choice of spatial prior.

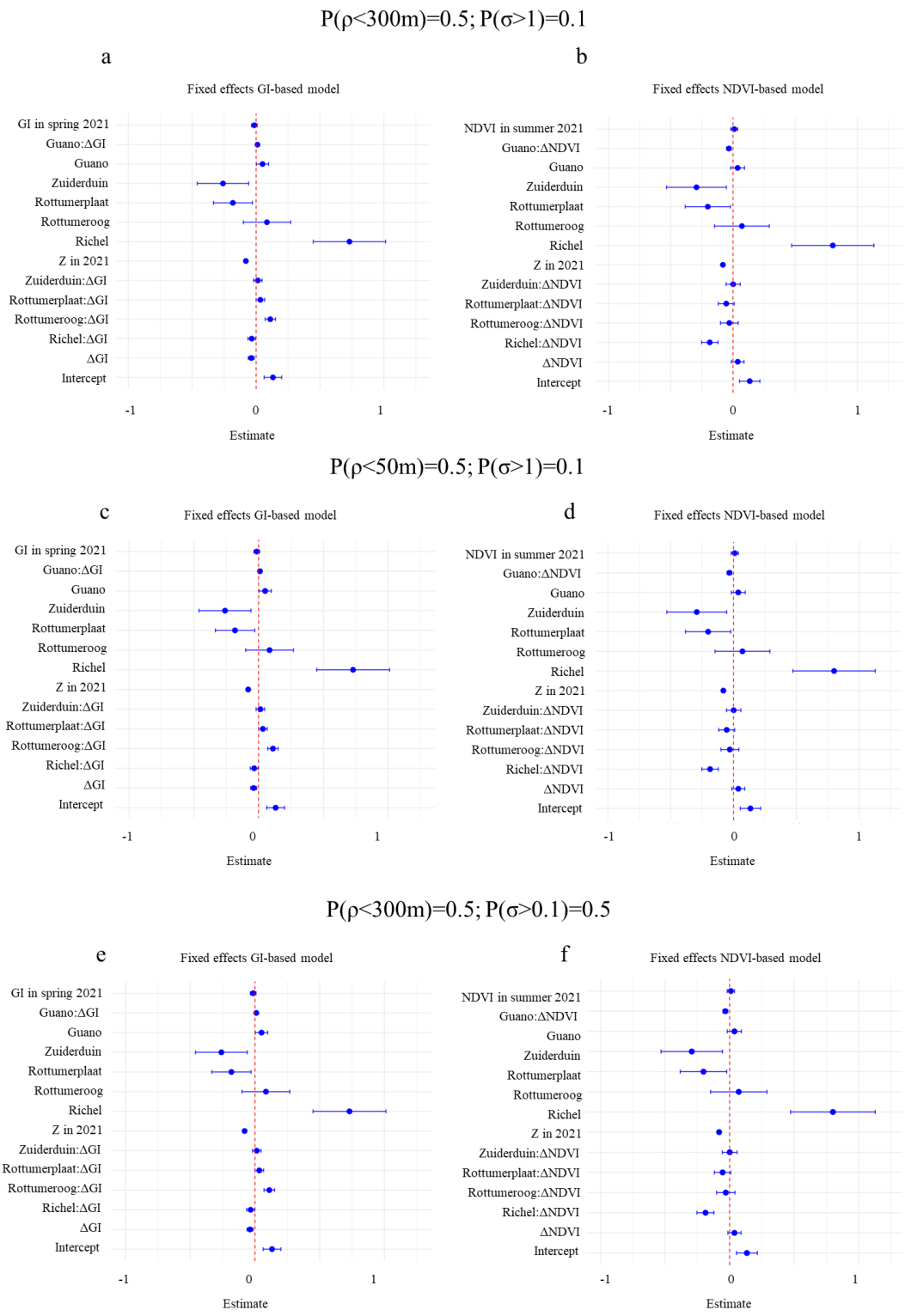

Fig. S6: Main-effect estimates (markers) with 95% credible intervals for GI-based (a, c and d) and NDVI-based (b ,d and f) spatial models for varying penalized complexity priors for the spatial field: reference (manuscript) prior (a &b), short-range sensitivity prior (c & d), and a weak spatial-effect prior (e & f).

S2.2 Mesh and Resolution Sensitivity Tests

Because INLA relies on integrated nested Laplace approximations rather than MCMC sampling, approximation stability was assessed through sensitivity analyses to mesh resolution. In addition to the mesh used in the main analyses (maximum edge length of 30 m within islands), we repeated model fitting using a finer internal resolution with a maximum edge length of 10 m.

While the finer mesh substantially increased computational cost, it had no meaningful effect on posterior estimates of fixed effects or their associated credible intervals for either the GI-based or NDVI-based models (Fig. S). This indicates that the spatial discretization was sufficiently fine to capture relevant spatial structure and that numerical inference was stable with respect to mesh resolution.

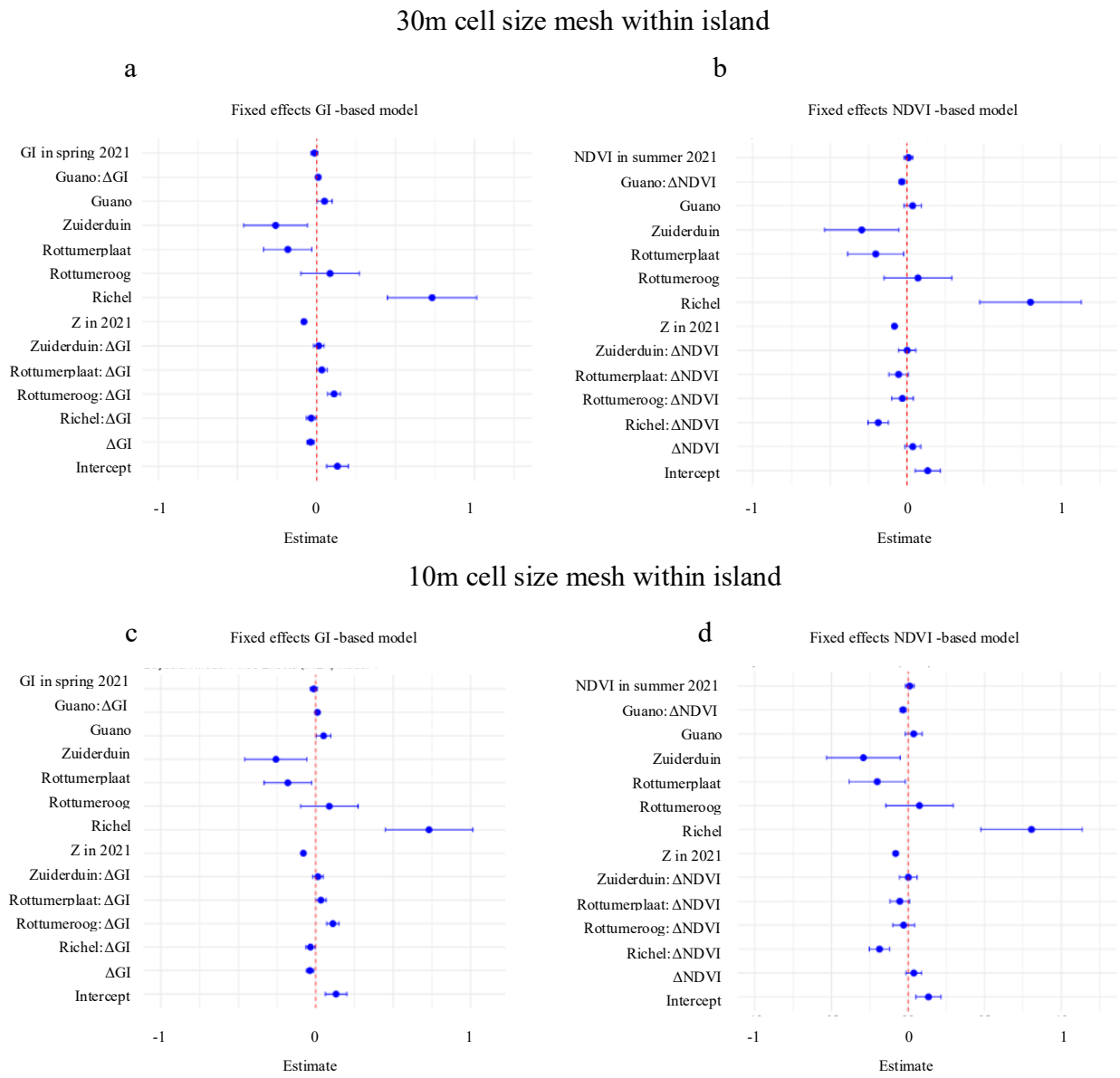

Fig. S7: Main-effect estimates (markers) with 95% credible intervals for (a) GI-based and (b) NDVI-based spatial models with a 30m cell size within islands as used in this manuscript, and additional runs with a 10m cell size within islands for (c) GI-based and (d) NDVI-based spatial models. All continuous predictors were z-standardised prior to modelling; coefficients therefore represent the effect of a one–standard-deviation change in each predictor.

S2.3 Mesh and Resolution Sensitivity Tests

We evaluated posterior predictive performance by comparing observed sediment bed level changes (ΔZ) with posterior predictive summaries from the fitted models. Fig. Fig. S shows observed ΔZ values plotted against posterior mean predictions for both the GI-based and NDVI-based models.

Both models showed strong agreement between observed and predicted values, with squared Pearson correlations (R^2) of 0.92 for each model, indicating that the models captured the dominant spatial and environmental patterns in bed level change. Deviations from the 1:1 line were primarily observed for extreme erosion values ($\Delta Z < -0.5$ m yr^{-1}), where both models tended to slightly underestimate erosion magnitude. These extreme values represent a small fraction of the total dataset (5000

observations) and suggest conservative behavior in the tails of the posterior predictive distribution rather than systematic model bias

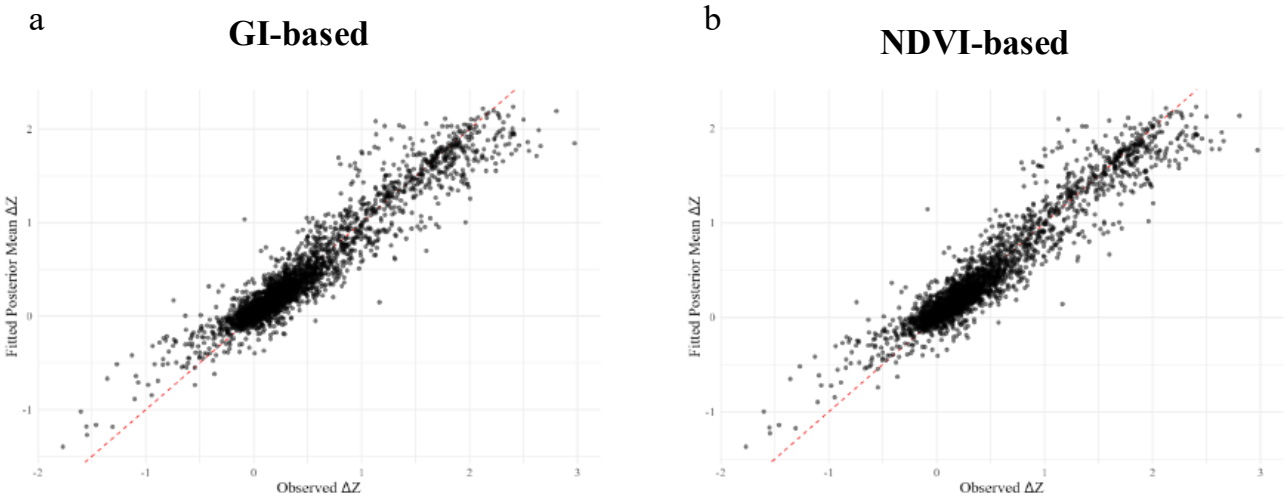

Fig. S8: Fitted posterior mean ΔZ predictions versus observed ΔZ values for the GI-based model (a) and the NDVI-based model (b).